JGR Atmospheres

RESEARCH ARTICLE
10.1029/2024JD042926

Impact of Boundary Layer Jets on Cold Pool Characteristics Observed From the 356-m High Shenzhen Meteorological Tower

Dong Fu[1], Yu Du[1,2,3,4], Chuying Mai[5], Minghua Li[6], and Chao Li[6]

[1]School of Atmospheric Sciences, Sun Yat-sen University, and Southern Marine Science and Engineering Guangdong Laboratory (Zhuhai), Zhuhai, China, [2]Heavy Rainfall Research Center of China, Wuhan, China, [3]Guangdong Province Key Laboratory for Climate Change and Natural Disaster Studies, Sun Yat-sen University, Zhuhai, China, [4]Key Laboratory of Tropical Atmosphere-Ocean System, Sun Yat-sen University, Ministry of Education, Zhuhai, China, [5]Key Laboratory of South China Sea Meteorological Disaster Prevention and Mitigation of Hainan Province, China Meteorological Administration, Haikou, China, [6]Meteorological Bureau of Shenzhen Municipality, and Key Laboratory of Severe Weather in South China, Shenzhen, China

Abstract The interaction between cold pools and low-level vertical wind shear plays an important role in the initiation and development of convection. However, the impact of the boundary layer jets (BLJs), with their unique low-level vertical wind shear structures and moisture transport properties, on cold pools remains incompletely understood. This study utilizes observations from the 356-m high Shenzhen Meteorological Tower to compare cold pool characteristics under BLJ and non-BLJ conditions during April to June from 2018 to 2020. A total of 54 cold pools are identified, with 26 influenced by BLJs. BLJ-related cold pools typically exhibit weaker average temperature drops, more pronounced decreases in specific humidity, and higher turbulence transport compared to those unrelated to BLJs. The enhanced moisture transport by BLJs constrains rainfall evaporation, resulting in weaker cold pools. In addition, the strong wind shear associated with BLJs promotes upward energy transport and turbulence, further weakening the intensity of cold pool. These distinctions are particularly pronounced in cold pools associated with mesoscale convective systems rather than individual convective cells. These findings provide valuable insights into the complex interactions among cold pools, BLJs, and convection in South China.

Plain Language Summary Cold pools are formed when precipitation evaporates and cools, and their leading edge can lift humid air and affect convection as they interact with low-level environmental flows. However, the characteristics of cold pools under the influence of boundary layer jets, featuring distinctive wind shear structures, are not well understood. The 356-m high Shenzhen Meteorological Tower in South China provides a valuable opportunity to examine the characteristics of cold pools in the presence of these jets. This study reveals that the jets tend to weaken cold pools due to their role in enhancing moisture transport and increasing vertical wind shear.

Key Points:

- Cold pool characteristics observed from the 356-m high Shenzhen Meteorological Tower vary depending on the presence of boundary layer jets (BLJs)
- Cold pools related to BLJs exhibit smaller temperature drops, larger humidity decreases, and enhanced turbulence
- Cold pools generated by MCSs are more strongly influenced by BLJs than those formed by individual convective cells

Supporting Information:

Supporting Information may be found in the online version of this article.

Correspondence to:

Y. Du,
duyu7@mail.sysu.edu.cn

Citation:

Fu, D., Du, Y., Mai, C., Li, M., & Li, C. (2025). Impact of boundary layer jets on cold pool characteristics observed from the 356-m high Shenzhen Meteorological Tower. *Journal of Geophysical Research: Atmospheres*, *130*, e2024JD042926. https://doi.org/10.1029/2024JD042926

Received 12 NOV 2024
Accepted 8 SEP 2025

1. Introduction

Cold pools are mesoscale areas of lower potential temperature air formed by evaporative cooling during precipitation accompanying downdrafts (Goff, 1976; Zipser, 1977). They are commonly found in convective precipitation regions over both land and sea (Zipser, 1977). The interaction between the leading edge of a cold pool and low-level environmental vertical wind shear can significantly influence the development and maintenance of convective squall lines (e.g., Bryan et al., 2006; Rotunno et al., 1988; Thorpe et al., 1982). Numerous studies have highlighted the crucial role of cold pools in convection and precipitation, as new convection can be triggered when a cold pool lifts warm and moist air at its leading edge (e.g., Feng et al., 2015; Marion & Trapp, 2019; Parker & Johnson, 2000; Purdom, 1976; Rotunno et al., 1988; Schlemmer & Hohenegger, 2015; Weisman et al., 1988). Schlemmer and Hohenegger (2014, 2015) and Torri et al. (2015) found that precipitation evaporation and advection can promote the formation of wider clouds and the transition from shallow to deep convection. Similarly, Khairoutdinov et al. (2009) further demonstrated that suppressing cold pools by deactivating precipitation evaporation reduces the occurrence of shallow and congestus clouds. Moreover, cold pools can impact air-sea interactions, enhancing fluxes between the atmosphere and ocean (e.g., Joseph et al., 2021; Simoes-Sousa et al., 2022).

Observations show that the characteristics of cold pools vary depending on oceanic or terrestrial environments and different synoptic conditions. For example, Kirsch et al. (2021), using data from a 280-m-high mast in Germany, found that summer cold pools typically caused a 2-m temperature decrease of 3.3 K and a specific humidity increase of 1 g kg^{-1}. In contrast, cold pools in the Netherlands generally display drier characteristic, with humidity decreasing and recovering within 1–2 hr (Kruse et al., 2022). Vogel et al. (2021) further reported that humidity increases both before and after the gust front onset, accompanied by a −0.9 K temperature change, while humidity decreases at the end of the front. In the northern Bay of Bengal, Simoes-Sousa et al. (2022) analyzed 456 cold pools across three moorings and observed dry characteristics, including an average temperature decrease of 2.8°C, a specific humidity reduction of 1 g kg^{-1}, and a recovery period ranging from 1.5 to 3.5 hr.

Cold pools in midlatitude continental regions tend to be more intense. van den Heever et al. (2021) investigated cold pools near Colorado using various instruments and found an average temperature perturbation of −8.0 K, a cold pool thickness spanning 200–2,300 m, and a wide range of vertical temperature profile. Similarly, other studies have also observed strong midlatitude cold pools with temperature drops up to 9 K (e.g., Engerer et al., 2008; Joseph et al., 2021). Grant et al. (2024) also noted significantly enhanced temperature variance at spatial scales of 5–15 km. These findings suggest that cold pools over tropical oceans tend to be weaker than those over midlatitude continents (Feng et al., 2015; Wang et al., 2019).

Various thermodynamic and dynamic factors can influence the properties of cold pools. Drager et al. (2020) conducted idealized cloud-resolving simulations, showing that lower soil moisture and enhanced latent cooling result in stronger and larger cold pools. Enhanced precipitation and evaporation drive stronger cold pools, highlighting how the atmospheric environment modulates them through its impact on evaporative cooling processes (e.g., Engerer et al., 2008; Tompkins, 2001). The dissipation of cold pools is further influenced by surface heat fluxes and turbulent entrainment, which are determined by surface temperature and wind speed (e.g., Gentine et al., 2016; Grant & Van Den Heever, 2016). Other numerical simulations also show that the ambient wind strength and shear affect the shape and movement of cold pools by modulating subsequent cooled downdrafts (e.g., Helfer & Nuijens, 2021; Parker, 1996). Investigating how these factors influence cold pools can enhance our understanding of cold pools evolution in different environments.

In the coastal regions of South China, cold pools often play a significant role in generating and sustaining heavy precipitation. The low-level outflow from cold pools induces moisture convergence, enhancing convection initiation during heavy rainfall (e.g., S. Li et al., 2021; H. Li et al., 2021; Su et al., 2023; Wang et al., 2014). The complex topography of South China can impede cold pool propagation, and interactions between the leading edge of cold pool and the low-level flow continuously generate new convection, promoting the development of mesoscale convective systems (MCSs) (Du et al., 2020; Zhang et al., 2022). Mai et al. (2023) investigated the dynamics of colliding cold pools during a heavy rainfall event in South China, discovering that the interaction between the cold pools prolonged the precipitation duration by affecting the development of squall lines.

During the pre-summer rainy season (April–June), the northward movement of southwesterly summer monsoon drives boundary layer jets (BLJs) over the northern South China Sea, transporting sufficient warm and moist air that promotes frequent convection in South China (e.g., Chen et al., 2017; Du & Chen, 2019a, 2019b; Li & Du, 2021). The BLJ is one type of low-level jet (LLJ). According to the classification proposed by Du et al. (2014) and Du and Chen (2019a), LLJs are broadly divided into two types: BLJs, typically located below 1 km, and synoptic-weather-related jets (SLLJs), generally found between 1 and 4 km. Given that cold pools primarily exist within the boundary layer, this study focuses on the impact of BLJs on cold pool characteristics. Du and Chen (2019a) demonstrated that BLJ events are frequent in this region during April–June, with maximum speeds at 950 hPa. BLJs are characterized by strong wind speeds (exceeding 10 m s^{-1} below 900 hPa), vertical wind shear, and horizontal vorticity, which influence heavy rainfall and nocturnal turbulence (IEC, 1999; Meng et al., 2004; Xu et al., 2023). Previous studies have shown that LLJs can alter cold pool structures. For example, Hitchcock and Schumacher (2020) found that non-unidirectional wind shear associated with LLJs can cause cold pools to expand on the side facing the jet and narrow on the opposite side. However, the detailed impacts of LLJs on cold pool characteristics remain insufficiently understood.

Pu et al. (2022) investigated an extreme rainfall event over coastal South China, revealing that BLJ-enhanced lifting of warm and moist air along a slow-moving cold pool outflow boundary contributed to the development and persistence of nocturnal rainstorm. Therefore, cold pools and BLJs collectively make significant

contribution to the evolution of MCSs in this region (Luo et al., 2017; Zhang et al., 2022). However, quantitative observations of cold pools in South China remain insufficient, limiting our understanding of their interactions with BLJs and their roles in heavy rainfall events. Mai et al. (2025) addressed this gap utilizing observational data from the Shenzhen Meteorological Tower to analyze the frequency and quantitative evolution of cold pools along the coast of South China. They found that cold pools occurred predominantly during early afternoon precipitation events from June to September, with average perturbation amplitudes falling between those characteristic of tropical and midlatitude environments (e.g., van den Heever et al., 2021; Vogel et al., 2021). In addition, they found that cold pools generated by MCSs were generally stronger (wind speed ∼28 m/s) and deeper (average depth ∼750 m) than those by individual convective cells (∼600 m depth). As previously mentioned, the South China region frequently experiences strong warm and humid airflows conveyed by BLJs, and cold pools might be significantly influenced by environmental moisture and strong winds. Therefore, it is essential to investigate the impacts of BLJs on cold pool characteristics.

Building upon Mai et al. (2025), this study further investigates how BLJs affect cold pool characteristics using Shenzhen Meteorological Tower observations. We also explore the environmental conditions surrounding cold pools to better understand the observed variations. The next section introduces the observational data and the methods used to identify cold pools and BLJs. In Section 3, we analyze the distinctions between BLJ-related and non-BLJ-related cold pools, along with comparisons of cold pools generated by different types of convection systems. The environmental conditions influencing cold pools are discussed in Section 4, followed by a summary and conclusions in Section 5.

2. Data and Methodology

2.1. Data

The study utilizes observational data obtained from a 356-m meteorological tower in Shenzhen, South China (113.89°E, 22.66°N), within the Pearl River Delta area. As the tallest meteorological gradient tower in Asia and the second tallest globally (He et al., 2022), the tower offers a unique platform for detailed vertical atmospheric observations. It records various key meteorological parameters, including temperature, wind speed, and relative humidity, across 13 gradient layers at the heights of 10, 20, 40, 50, 80, 100, 150, 160, 200, 250, 300, 320, and 350 m. Pressure is measured at three specific heights (50, 100, and 300 m). These data are collected at a high temporal resolution of 5 min, enabling the fine-scale monitoring of cold pool dynamics. Additionally, the eddy covariance (EC) data used in this study were obtained from a flux observation system installed on the Shenzhen Meteorological Tower at 10 and 320 m above the ground level where the sensors are located. The raw 10-Hz time series data were processed into 30-min averages following a standard postprocessing routine (Lan et al., 2018, 2019), which included (a) removal of spikes and high-frequency noise; (b) replacement of outliers exceeding five times the standard deviation using linear interpolation; (c) calculation of mean values, variances, and covariances using 30-min unweighted block averaging; and (d) data quality control following the approach of Foken et al. (2005).

For this analysis, we employ observational data during the pre-summer rainy season (April–June) spanning the 3 years from 2018 to 2020. Bias correction is applied to address the overestimation of relative humidity in the near-saturated states caused by sensors using the observational tower data between 2018 and 2020 (Mai et al., 2023). For physical consistency, all relative humidity values exceeding 100% were capped at 100%. To accurately assess humidity variations within cold pools, specific humidity (q, kg kg^{-1}) is calculated using relative humidity, pressure, and saturation vapor pressure, with the latter computed based on the formulation by Alduchov and Eskridge (1996).

To identify cold pools generated from convection, we use radar data from the China Meteorological Administration, with a temporal resolution of 6 min. Furthermore, the fifth-generation European Center for Medium-Range Weather Forecast atmospheric reanalysis (ERA5, Hersbach et al., 2020) is employed to identify BLJ events and analyze the associated environmental conditions. ERA5 data have a horizontal resolution of 0.25° × 0.25° and a temporal resolution of 1 hr.

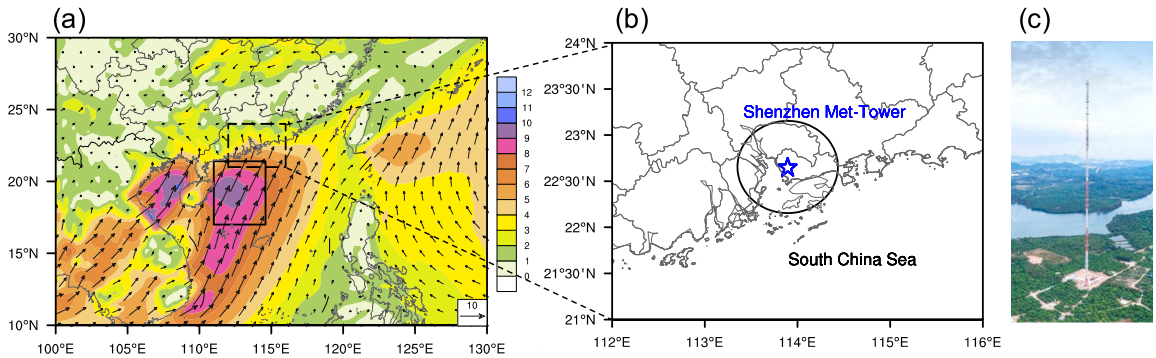

Figure 1. (a) Horizontal wind distribution at 950 hPa (m s^{-1}) during heavy rainfall events (daily precipitation exceeding 50 mm near the Shenzhen Meteorological Tower) in the pre-summer rainy season. The solid black box indicates the region selected to define boundary layer jet events. (b) The location of the Shenzhen Meteorological Tower marked by a blue star, and the circle denotes a range within a radius of 0.5° from the tower. (c) A photo of the tower.

2.2. Identification of BLJs

Following the criteria outlined by Du & Chen. (2019a) and Du et al. (2014), BLJs are identified based on the following conditions:

1. The maximum wind speed below 900 hPa exceeds 10 m s^{-1}.
2. The wind speed decrease of at least 3 m s^{-1} occurs between the low-level wind maximum and either a wind minimum or below the 600 hPa level.

BLJ events are defined using ERA5 reanalysis data if more than 20% of the grid cells within the solid black box in Figure 1 meet the above BLJ criteria, and the prevailing wind direction is southwesterly, which plays a critical role in moisture transport and precipitation over South China. This black box is the region related to the high frequency of BLJ locations over the northern South China Sea (Du et al., 2022), where these jets are key contributors to inland moisture delivery and significantly influence heavy rainfall events in South China during the pre-summer rainy season (Du & Chen, 2018, 2019b).

2.3. Identification of Cold Pools

Previous observational studies have primarily adopted specific temperature decrease criteria to identify cold pools (Joseph et al., 2021; Simoes-Sousa et al., 2022; Vogel et al., 2021). In this study, we employ an objective identification method following Kirsch et al. (2021) and Mai et al. (2025). The temperature at the lowest observational level (10 m) serves as the threshold for detecting cold pool events. A cold pool event is defined when the 10-m temperature decreases by more than 2°C ($\Delta T_{10} \leq -2$°C) compared to 20 min earlier. The onset of a cold pool (t_0) occurs when the temperature first decreases by at least 0.5°C from the previous measurement (taken 5 min earlier). Any further temperature decreases within the following 60 min are considered part of the same event.

To confirm that the selected cold pools are driven by convection, we require the maximum composite radar reflectivity to exceed 20 dBZ within a 0.5° radius of the Shenzhen Meteorological Tower during the 30 min prior to t_0 (Figure 1b). Sensitivity tests using alternative parameters, such as a smaller radius (e.g., 0.25°) and a higher reflectivity threshold (e.g., 35 dBZ), confirm that the cold pool identification method is robust and not overly sensitive to the choice of threshold values. Events with missing data within 30 min before or 60 min after t_0 are excluded from the analysis to ensure data integrity.

Cold pools that coincide with BLJ events are categorized as BLJ-related cold pools, while those occurring when no BLJ is present are classified as non-BLJ-related cold pools. A total of 54 events satisfying the defined criteria were identified, comprising 26 BLJ-related cold pools and 28 non-BLJ-related cold pools (Figures S1–S26 in Supporting Information S1). Notably, the cold pool selection process is based solely on observed temperature variations and does not exclude cooling events associated with synoptic-scale cold-frontal passages. Manual inspection revealed a lower frequency (14.8%) of cold pool events accompanied by cold fronts, and these events were directly influenced by convection near the front rather than by the cold front itself.

To assess the statistical significance of differences between BLJ-related and non-BLJ-related cold pool distributions, Welch's *t*-test was employed. This test is well-suited for comparing means between two groups with unequal variances and sample sizes and is commonly used in environmental studies to assess the significance of differences in meteorological conditions (e.g., Gaal et al., 2024; Lavers et al., 2015). Similarly, an *F*-test was applied to assess the significance in the magnitude of variability in EC between the two types of cold pools. In this study, a p-value threshold of 0.1 was adopted to indicate statistical significance, corresponding to a 90% confidence level.

2.4. Classification of Convective Systems

To better explore the effect of BLJs on the characteristics of cold pools generated by different convective systems, cold pools are further classified into two categories based on their parent convection systems: MCSs and individual convective cells. This classification is determined by examining the dominant convective structure observed within 30 min prior to the passage of cold pools over the Shenzhen Meteorological Tower. The convective system located closest to the tower during this period is identified as the parent system of the cold pool.

Following previous studies (Parker & Johnson, 2000; Schiro & Neelin, 2018), MCSs are defined as the contiguous-precipitation regions with reflectivity exceeding 30 dBZ and spanning at least 100 km in any direction horizontally. In contrast, individual convective cells also meet the 30 dBZ reflectivity threshold but smaller than 100 km in a horizontal scale. When using a 10-km threshold, the fundamental characteristics of different types of cold pools remain consistent. This classification method has been successfully adopted in previous studies over south China, demonstrating its applicability and effectiveness in this region (e.g., S. Li et al., 2021; H. Li et al., 2021; Mai et al., 2025).

In this study, the sample is roughly balanced between the two categories: 15 BLJ-related and 11 non-BLJ-related cold pools are associated with MCSs, while 11 BLJ-related and 17 non-BLJ-related cold pools are linked to individual convective cells.

Radar-based identification can capture smaller and shorter-lived storms but involves a degree of subjectivity, whereas objective tracking algorithms may underestimate such systems due to threshold constraints. This trade-off leaves some uncertainty in the classification and warrants further examination in future work.

2.5. Moisture Fluxes and Vapor Transport

To assess moisture transport associated with BLJ events, we calculate vertically integrated water vapor fluxes (kg $s^{-1}m^{-1}$) according to Du et al. (2020):

$$Q = \frac{1}{g}\int_{p_0}^{p_1} qV dp$$

Here, q represents the water vapor mixing ratio, V is the wind velocity perpendicular to the lateral boundaries, and g is the gravitational constant. The pressure levels p_1 and p_0 correspond to 900 and 1,000 hPa, respectively. The integrated vapor transport (plane integration of water vaper fluxes, kg s^{-1}) between two points x_1 and x_2 is calculated as follows:

$$\overline{Q_{x_1 x_2}} = \int_{x_1}^{x_2} Q\, dx$$

Subsequently, the net moisture fluxes within a specific area are given by

$$Q_{\text{net}} = \overline{Q_{\text{south\_plane}}} + \overline{Q_{\text{north\_plane}}} + \overline{Q_{\text{east\_plane}}} + \overline{Q_{\text{west\_plane}}}$$

3. Comparison of BLJ-Related and Non-BLJ-Related Cold Pools

3.1. General Characteristics of BLJ-Related and Non-BLJ-Related Cold Pools

The vertical variations in perturbations due to BLJ-related and non-BLJ-related cold pools are compared in Figure 2. Perturbations are defined as the differences between extreme values within 60 min after t_0 and the

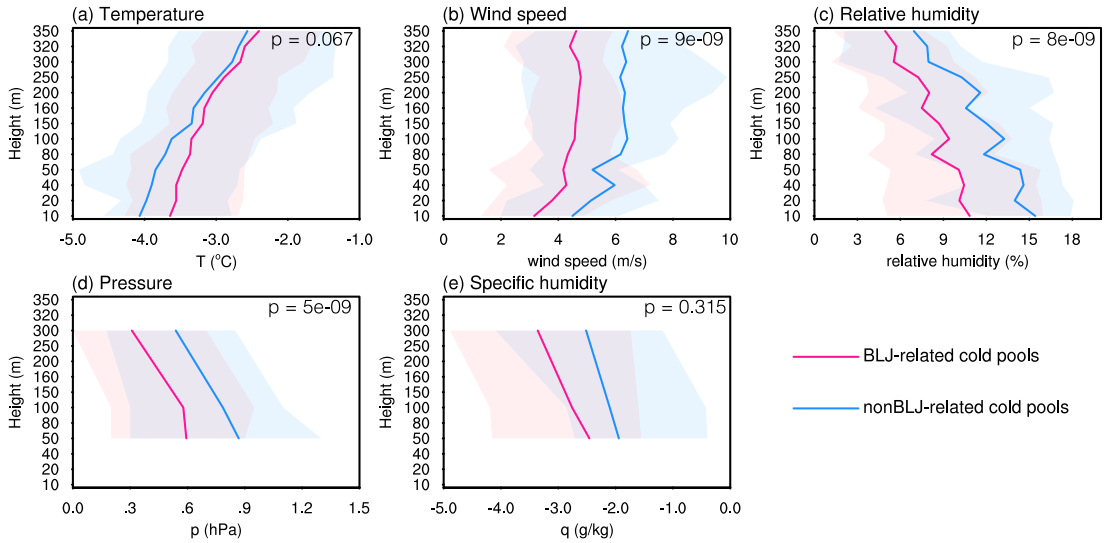

Figure 2. Vertical distributions of perturbations in (a) temperature (°C), (b) wind speed (m s^{-1}), (c) relative humidity (%), (d) pressure (hPa), and (e) specific humidity (g kg^{-1}) during cold pool passages at the Shenzhen Meteorological Tower. Blue and pink lines represent non-BLJ-related and BLJ-related cold pools, respectively. The shaded areas represent the interquartile range (25%–75%), and the solid line shows the mean values. *P*-values from Welsh's *t*-test are used to determine the statistical significance between BLJ-related and non-BLJ-related cold pools.

median state within 30 min before t_0, thereby representing changes associated with cold pool passage. When BLJ-related cold pools pass, the 10-m temperature exhibits an average decrease of 3.6°C (Table 1), with over 25% of events experiencing a drop of 4.3°C (Figure 2a). In contrast, for non-BLJ-related cold pools, the average decrease at 10 m is 4.1°C, with over 25% of events observing drops of 4.6°C. The average temperature perturbations for BLJ-related cold pools are vertically consistently smaller than those of the non-BLJ-related cold pools. These differences between the two types of cold pools are statistically significant at the 90% confidence level (*p*-value <0.1). Compared to non-BLJ-related cold pools, the temperature in BLJ-related events decreases less sharply with height, indicating a relatively less stability.

Figure 3 further illustrates the temporal evolution of perturbations. As shown in Figures 3a and 3b, BLJ-related cold pools sustain cooling at higher layers (200–300 m), with the minimum temperature perturbations occurring approximately 25 min after the passage. Near the surface (10–40 m), cooling persists for about 30 min, suggesting a longer cooling duration at lower levels. In contrast, non-BLJ-related cold pools exhibit more prolonged cooling across all levels, lasting nearly 35 min before gradually transitioning into a slower recovery phase. The temporal evolution further indicates that non-BLJ-related cold pools cool the lower layers (10–40 m) more rapidly than BLJ-related ones (Figure 3c), with their influence persisting for more than 60 min after passage at the Shenzhen Meteorological Tower.

As cold air accumulates within the cold pool, surface pressure increases accordingly. The average cooling rate of BLJ-related cold pools is less than that of non-BLJ-related ones, resulting in a significantly smaller average pressure increase at three layers, with changes of 0.6 and 0.9 hPa at 50 m, respectively (Figures 2d and Table 1). In addition, over 25% BLJ-related (non-BLJ) cold pools exhibit pressure increases of 0.9 hPa (1.3 hPa) at 50 m. The

Table 1
Mean Perturbation Values at Selected Heights for Non-BLJ-Related and BLJ-Related Cold Pools

	Temperature (℃) (BLJ/non-BLJ)	Pressure (hPa) (BLJ/non-BLJ)	Wind speed (m/s) (BLJ/non-BLJ)	Specific humidity (g/kg) (BLJ/non-BLJ)	Relative humidity (%) (BLJ/non-BLJ)
10 m	−3.6/−4.1		3.2/4.5		10.8/15.5
50 m	−3.5/−3.9	0.6/0.9	4.2/5.2	−2.4/−1.9	10.4/14.7
100 m	−3.5/−3.6	0.6/0.8	4.6/6.4	−2.8/−2.1	9.6/13.5
300 m	−2.7/−2.8	0.3/0.5	4.7/6.4	−3.4/−2.5	5.5/8.4

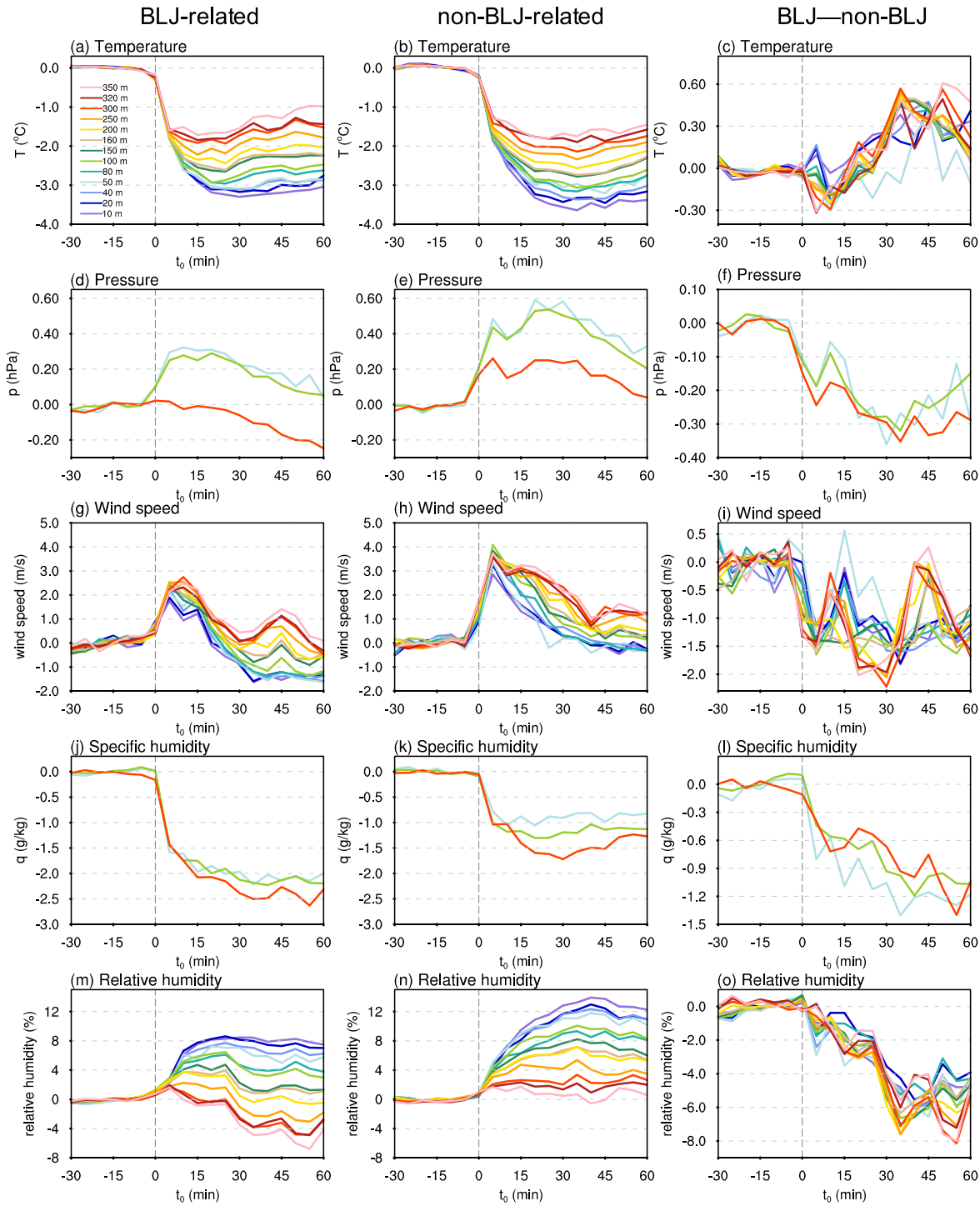

Figure 3. Mean temporal evolution of perturbations at different heights (represented by different colored lines) before and after the cold-pool-front passage at t_0. The first and second columns represent BLJ-related and non-BLJ-related cold pools, respectively, and the third column represents the differences between the two groups (BLJ-non-BLJ).

shorter cooling duration observed in BLJ-related cold pools leads to a correspondingly briefer increase in pressure, lasting only 10 min, compared to 20 min for non-BLJ-related cold pools at 50 m (Figures 3d and 3e). Similar differences in pressure evolution are observed across other vertical levels (Figure 3f).

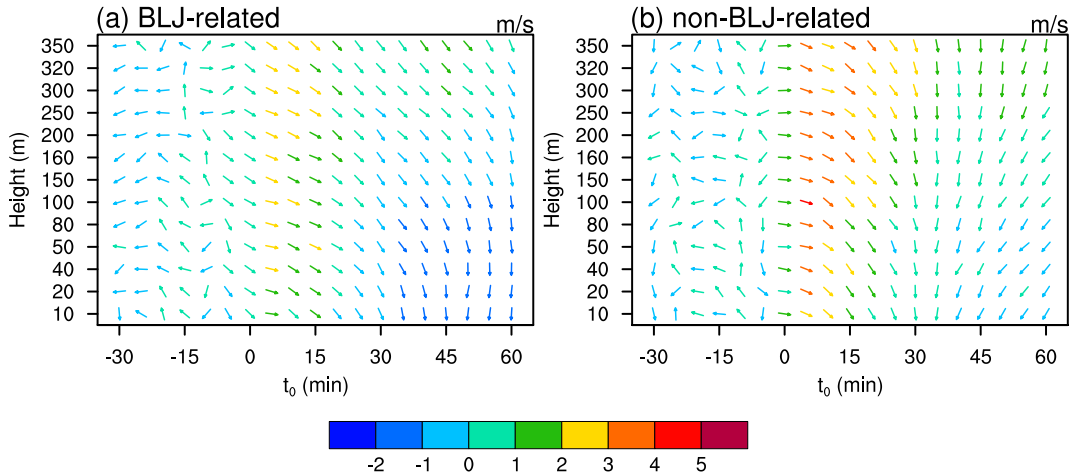

Figure 4. Mean temporal evolution of perturbations in the horizontal wind field (m s^{-1}, colored by wind speed perturbations) at different heights before and after the cold-pool-front passage at time t_0 for (a) BLJ-related and (b) non-BLJ-related cold pools.

As the cold pool passes the Shenzhen Meteorological Tower, the gust front at its leading edge brings strong winds. Figure 2b illustrates that wind speed amplifies with height relative to the background wind field (i.e., the median wind speed within 30 min prior to the cold pool passage) due to the friction near the surface. The average wind speed increase in BLJ-related cold pools is significantly lower than that in non-BLJ-related cases at all layers. Particularly, approximately 75th percentile of BLJ-related cold pool wind speed increase is even lower than the mean wind speed increase of non-BLJ-related events. This pronounced discrepancy may be attributed to the southwesterly wind direction of the BLJs and the southeastward propagation of most cold pools, which can impede and slow down the spread of BLJ-related cold pools. As shown in Figure 4, the enhancement of northwesterly winds associated with the gust front at 5 min after t_0 clearly indicates the southeastward propagation of cold pools. However, for BLJ-related cold pools, the gust front intensification is weaker due to the opposing influence of the strong southwesterly background flow brought by the BLJs (Figures 1a and 4a). Specifically, the 10-m wind speed exhibits a larger change of 4.5 m s^{-1} for non-BLJ-related cold pools compared to BLJ-related ones (3.2 m s^{-1}).

Moreover, the growth of wind speeds begin to slow around 5 min after t_0 (Figures 3g and 3h). The BLJ-related wind speed variations are more pronounced in lower layers (10–80 m), resulting in values after 20 min that are lower than the unperturbed states (Figure 3g). Upper-level wind speed exhibits markedly different temporal variations in BLJ-related versus non-BLJ-related cold pools (Figure 3i). Around 50 min (40 min) after t_0, the near-surface horizontal wind field associated with BLJ-related (non-BLJ-related) cold pools starts to shift to a northeasterly wind, indicating the passage of low-level backflow behind the gust front (Figure 4), likely induced by the surface friction (Goff, 1976).

Specific humidity shows a decreasing tendency in most cold pools after their passage, with the mean reduction in BLJ-related cold pools being slightly larger than that of non-BLJ-related ones, although the difference is not statistically significant (Figure 2e). At 50 m, the mean specific humidity decrease is 2.4 g kg^{-1} for BLJ-related cold pools and 1.9 g kg^{-1} for non-BLJ-related ones (Table 1). This reduction increases with height, reaching 3.4 and 2.5 g kg^{-1} at 300 m, respectively. At the 25th percentile, BLJ-related (non-BLJ-related) cold pools show a reduction of −5.0 g kg (−4.1 g kg) at 300 m. The increase or decrease of specific humidity can be attributed to two processes: rainfall evaporation, which moistens the cold pools, and the downward transport of dry and cold air from upper layers, which dries them. The observed decrease in specific humidity in most cold pools indicated that the latter dominates. The reduction of specific humidity in the BLJ-related cold pools continues for nearly 35–40 min, longer than the 25–30 min duration in non-BLJ-related cold pools (Figures 3j, 3k and 3i), indicating a stronger drying effect in BLJ-related cold pools. This will be further discussed in Section 4.

Both temperature and specific humidity can influence relative humidity, though temperature has a greater impact. Therefore, relative humidity increases less in BLJ-related cold pools, with values of 10.8% at 10 m and 5.5% at 300 m, significantly compared to non-BLJ-related ones (15.5% at 10 m, 8.4% at 300 m) (Figures 2c and Table 1). In addition, the temporal evolution of relative humidity also varies significantly with height. In BLJ-related cold pools, relative humidity at lower layers increases with time after t_0, while at higher layers, it decreases following an initial rise (Figures 3m). This contrasts with non-BLJ-related cold pools, where relative humidity increases steadily across all layers (Figures 3n and 3o). These variations in BLJ-related cold pools may be attributed to a greater reduction in specific humidity and a smaller temperature decrease at higher layers.

From Figure 3a, it is evident that the temperature influenced by the BLJ-related strong winds exhibits a periodic oscillation of about 15 min, especially at higher layers. This is further supported by pronounced power observed in wavelet analysis (not shown). Such oscillation might be ascribed to the turbulent oscillation resulting from the interaction between the cold pool and ambient environment (Zhang et al., 2023).

Previous studies have shown that the gust front passages typically induce significant changes on the mechanisms of turbulence generation and the thermodynamic structure of the atmospheric boundary layer (Chowdhuri et al., 2021; Han et al., 2020; Xie et al., 2022). Based on this, the temporal evolution of EC as the gust front passes through is analyzed (Figure 5). It should be noted, however, that the EC method assumes stationarity and horizontal homogeneity, which are not satisfied in the cold pool environment. The nonstationary and advective characteristics of cold pools can significantly distort flux estimates, even to the extent of altering their sign. Therefore, our analysis does not emphasize the exact flux magnitudes, but rather the qualitative evolution of surface-layer turbulence before, during, and after the cold pool passage, especially under the influence of strong low-level wind shear associated with BLJs.

The passage of cold pools leads to surface cooling, thereby reducing sensible heat flux (SH). Consequently, temperature decreases more for non-BLJ-related cold pools, enhancing the significantly SH loss to -51.6 w m^{-2} at 10 m, 30 min after t_0 (Figures 5a and 5b). It is apparent that BLJ-related cold pools experience less SH loss (-37.8 w m^{-2} at 320 m). Furthermore, energy is predominantly transported upward following the gust fronts and enhanced turbulence. Momentum flux (TAU) is notably higher for BLJ-related cold pools than for non-BLJ-related cold pools, particularly in the higher layers (320 m), with peak values (1.4 kg/(m s^2) and 1.0 kg/(m s^2), respectively) observed 30 min after t_0 (Figures 5c and 5d). This enhancement is attributed to stronger vertical wind shear in BLJ events, measured at 0.0176 s^{-1} between 10 and 320 m, compared to 0.0119 s^{-1} in non-BLJ-related events. After 60 min past the gust front passage, TAU rapidly declines at both heights.

Turbulent kinetic energy (TKE), an indicator of turbulence intensity, also increases markedly in response to enhanced wind shear and gust front strength. As shown in Figures 5g and 5h, TKE intensifies in both types of cold pools during the gust front passage. For BLJ-related cold pools, TKE at 320 m is 1.7 m^2 s^{-2} 30 min before the cold pool passage, then rapidly increases to 6.0 m^2 s^{-2} in the following 60 min. For non-BLJ-related cold pool, the strong gust front also leads to higher TKE (4.7 m^2 s^{-2} at 320 m) at 30 min after t_0. Overall, TKE exhibits substantial fluctuations, and the differences between the two types of cold pools are statistically significant. Similarly, the strong wind shear and high wind speeds of BLJs lead to a larger friction velocity (U*), which characterizes the transport of the mechanical turbulence (Figures 5e and 5f). In BLJ-related cold pools, U* reach a higher value of 1.0 m s^{-1} at 320 m. Additionally, TAU, TKE, and U* exhibit lager values at 320 m around 30 min after t_0, roughly coinciding with the onset of temperature recovery (Figures 3a and 3b).

These findings suggest that the enhanced turbulent momentum and energy exchange accelerate the dissipation of cold pools, particularly in BLJ-related cold pools, thereby hindering their development (Figure 3a). This is consistent with the observations of Ross et al. (2004), who found that the strong heat flux accelerates the demise of cold pools by enhancing turbulent instability.

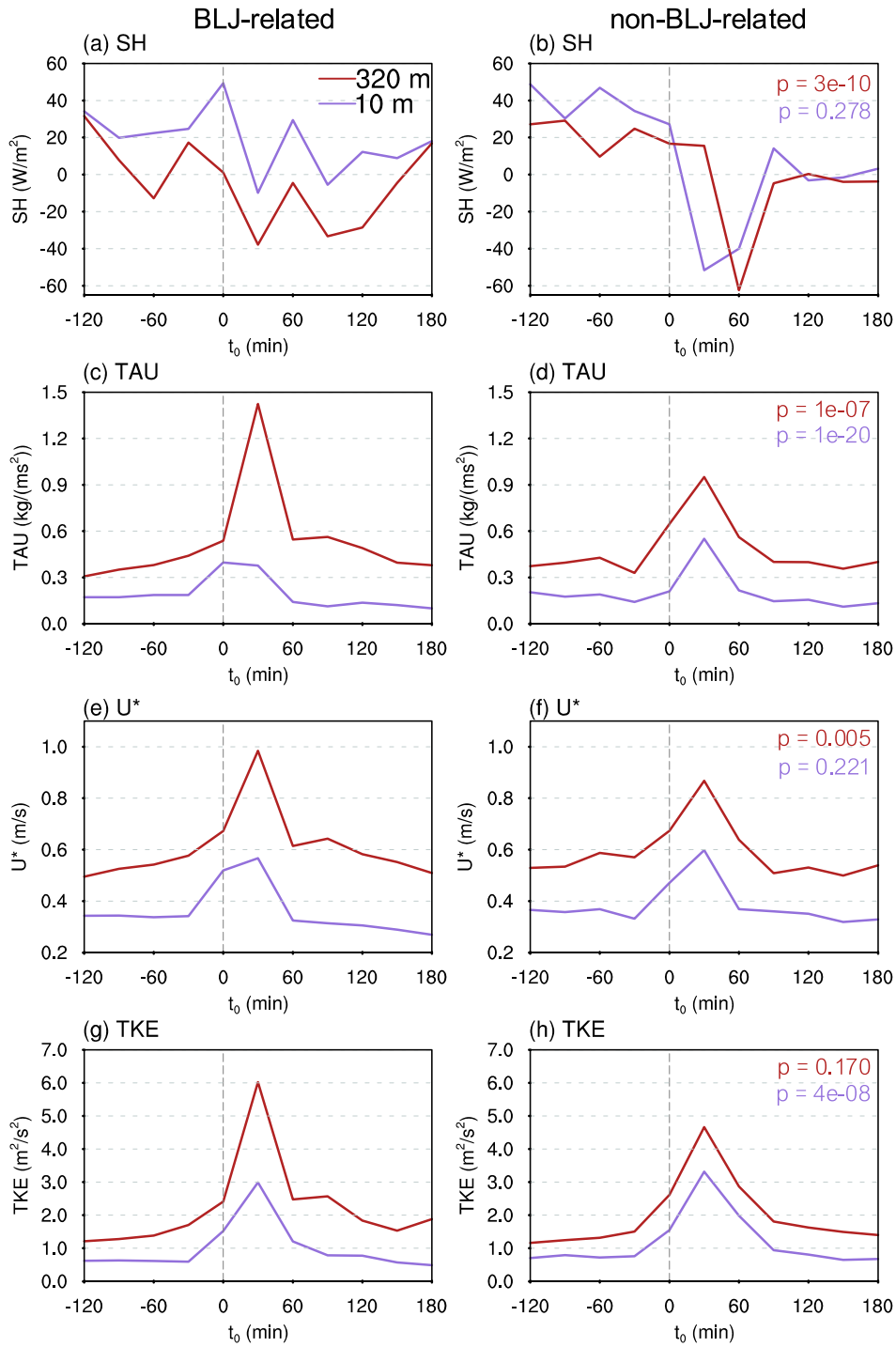

Figure 5. Temporal evolution of (a, b) sensible heat flux (w m^{-2}), (c, d) momentum flux (kg m^{-1} s^{-2}), (e, f) friction velocity (m s^{-1}), and (g, h) turbulent kinetic energy (m^2 s^{-2}) at 10 and 320 m heights before and after the cold-pool-front passage at time t_0. The left and right columns represent BLJ-related and non-BLJ-related cold pools, respectively. P-values from the *F*-test are used to determine the statistical significance between BLJ-related and non-BLJ-related cold pools. Red and purple represent results at 320 and 10 m heights, respectively.

3.2. Cold Pools Generated From MCSs and Individual Convective Cells

Previous studies (e.g., Engerer et al., 2008; Vogel et al., 2021) have suggested varying responses of cold pools during different stages of the convective system life cycle. However, further investigation is needed to understand the behaviors of cold pools generated by different convective modes under the influence of BLJs, including MCSs and individual convective cells.

The distributions and temporal evolutions of perturbations in cold pools from MCSs closely resemble the general characteristics of all cold pools (Figure 6). However, a more significant disparity exists between BLJ-related and non-BLJ-related cold pools in the magnitude of various perturbations across 13 heights, suggesting a greater impact of the BLJs on MCSs cold pools.

Figure 6a shows that the 10-m mean temperature drop is 4.1°C for BLJ-related cold pools and 5.3°C for non-BLJ-related cold pools from MCSs, with a difference of over 1° (Table 2). This difference remains pronounced at higher altitudes, with −3.3°C and −4.3°C change at 300 m, respectively. Notably, 75% of BLJ-related cold pools exhibit temperature decreases of less than 4.4°C. The mean temperature perturbation for MCSs cold pools in this study is smaller than the temperature deficits reported by Engerer et al. (2008), which ranged from −9.5 to −5.4 K in Oklahoma. Over time, the BLJ-related cold pools show a temperature decrease of 3.8°C at 10 m at 30 min after t_0 (Figure 6b), while the non-BLJ-related cold pools experience a larger drop, reaching 5.0°C at 35 min (Figure 6c). This indicates more sustained cooling in the absence of a BLJ.

In terms of pressure, the average rise in BLJ-related cold pools from MCSs (e.g., 0.8 hPa at 50 m) is smaller than that of non-BLJ-related ones (e.g., 1.6 hPa at 50 m), with over 25% of the latter showing a pressure increase as high as 2.5 hPa at 50 m (Figure 6d). In addition, the pressure rise lasts longer in non-BLJ-related cold pools (Figures 6e and 6f). Wind speed perturbations are significant for both types of cold pools, exceeding 4.9 m s^{-1} at 10 m on average. However, BLJ-related cold pools exhibit less changes with height, with a 300-m mean value of 5.9 m s^{-1}, compared to 10.8 m s^{-1} for non-BLJ-related cold pools at the same altitude (Figure 6g). At the higher level (320 m), more than 25% of non-BLJ-related cases exhibit a stronger wind speed increase up to 16.2 m s^{-1}. The wind speed anomalies for BLJ-related cold pools reach their maximum of 3.6 m s^{-1} at 200 m at 20 min (Figure 6h), which is lower than the 7.8 m s^{-1} peak observed at 300 m at 5 min for non-BLJ-related cold pools (Figure 6i).

The specific humidity perturbation is greater in BLJ-related cold pools from MCSs, with average values of −3.2 g kg^{-1} at 50 m, compared to −2.6 g kg^{-1} for non-BLJ-related events (Figure 6j). Specific humidity decrease in BLJ-related cold pools can reach up to 3.4 g kg^{-1} at 35 min after t_0 (Figure 6k), exceeding the 2.8 g kg^{-1} decrease at 30 min for non-BLJ-related cold pools (Figure 6l). Relative humidity at 10-m increases by an average of 9.5% in BLJ-related cold pools, while non-BLJ-related events experience a larger increase of 16.8% (Figure 6m). Moreover, a quarter of BLJ-related (non-BLJ-related) relative humidity at 10 m increase exceeding 14.9% (22.8%). The temporal evolution of relative humidity (Figures 6n and 6o) closely aligns with the general characteristic of all cold pools (Figures 3e and 3j).

Similar analyses were conducted for cold pools from individual convective cells, indicating a more limited influence of BLJs on these cold pools (Figure 7). Compared to the MCSs-generated cold pools, the differences in temperature perturbations between BLJ-related and non-BLJ-related cold pools from individual convective cells are less pronounced in all heights (Figure 7a). Despite this, the cooling effect of BLJ-related cold pools remains weaker, with a temperature decrease of 3.1°C at 10 m, compared to 3.4°C for non-BLJ-related ones, and the duration of cooling is shorter (Figures 7b and 7c, Table 3). In addition, the pressure differences between BLJ-related and non-BLJ-related cold pools are minimal (nearly 0.4 hPa at 50 m), suggesting comparable intensities (Figures 7d–7f).

The wind speed increase in the two types of cold pools from individual convective cells is significantly distinct, with 10-m averages of 3.5 m s^{-1} for non-BLJ-related cold pools and 1.7 m s^{-1} for BLJ-related ones (Figure 7g). Although BLJ-related cooling exhibits similarities with non-BLJ-related cold pools, specific humidity declines more in BLJ-related cold pools, with means of −1.7 g kg^{-1} at 50 m compared to −1.1 g kg^{-1} for non-related cold pools (Figure 7j). Notably, the recovery of specific humidity is slower in BLJ-related cold pools (Figures 7k and 7l). As a result of combined temperature and specific humidity effects, the relative humidity increase at 10 m differs significantly between the two cases, averaging 11.8% for BLJ-related cold pools and 15.5% for non-BLJ-

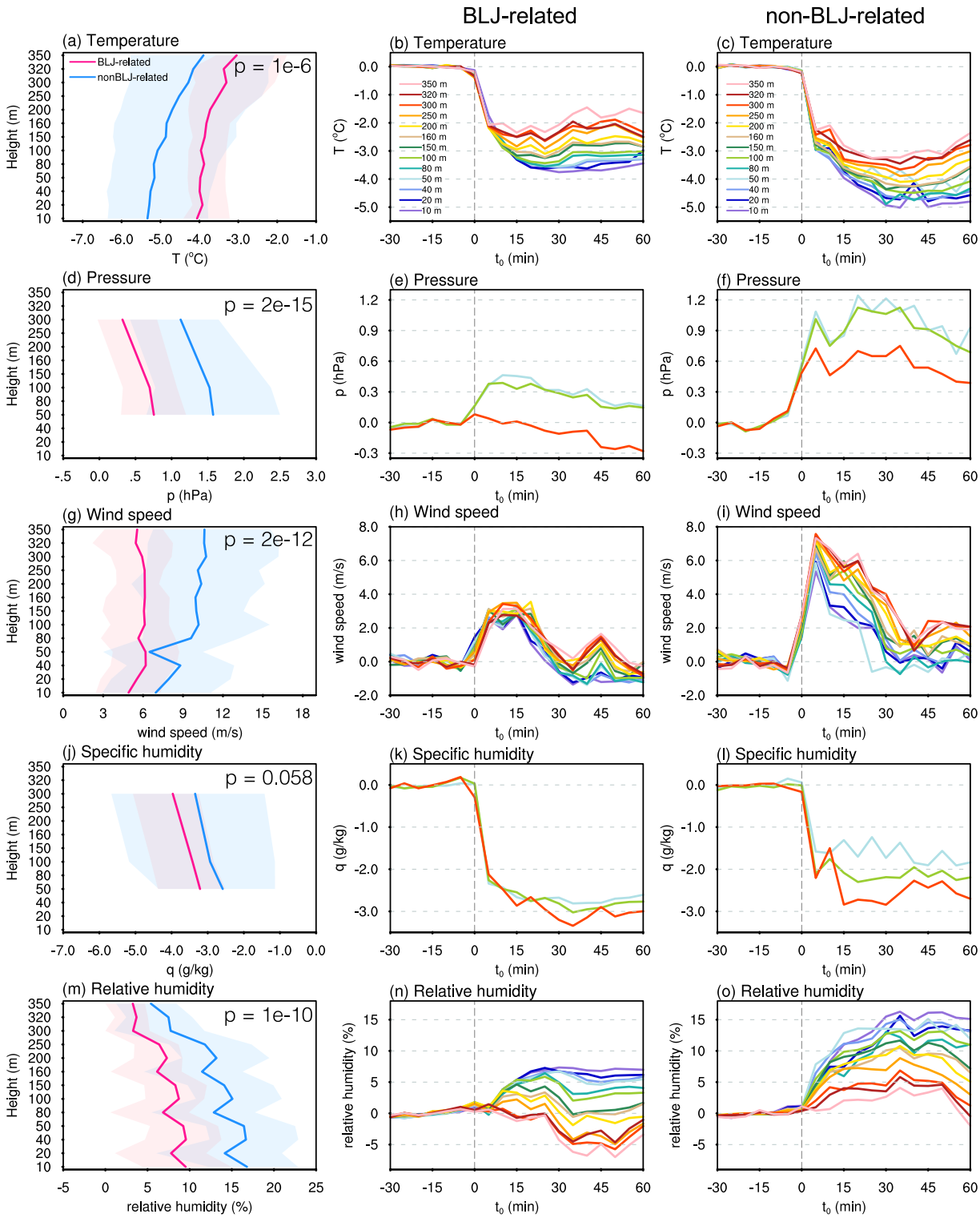

Figure 6. Vertical distributions and mean temporal evolution of the perturbations in (a–c) temperature (°C), (d–f) pressure (hPa), (g–i) wind speed (m s^{-1}), (j–l) specific humidity (g kg^{-1}), and (m–o) relative humidity (%) for cold pools generated from MCSs. The second and third columns represent BLJ-related and non-BLJ-related cold pools, respectively. P-values from Welsh's *t*-test are used to determine the statistical significance between BLJ-related and non-BLJ-related cold pools.

Table 2
Mean Perturbation Values at Selected Heights for Non-BLJ-Related and BLJ-Related Cold Pools Generated From MCSs

	Temperature (°C) (BLJ/non-BLJ)	Pressure (hPa) (BLJ/non-BLJ)	Wind speed (m/s) (BLJ/non-BLJ)	Specific humidity (g/kg) (BLJ/non-BLJ)	Relative humidity (%) (BLJ/non-BLJ)
10 m	−4.1/−5.3		4.9/7.0		9.5/16.8
50 m	−4.0/−5.2	0.8/1.6	6.2/6.5	−3.2/−2.6	9.2/16.4
100 m	−3.9/−5.1	0.7/1.5	6.1/10.2	−3.4/−2.9	8.7/15.1
300 m	−3.3/−4.3	0.3/1.1	5.9/10.8	−4.0/−3.3	3.3/7.7

related ones (Figure 7m). Likewise, relative humidity increases over time in the lower layers of BLJ-related cold pools, while it decreases in the upper layers (Figure 7n). This pattern still contrasts with non-BLJ-related cold pools, where relative humidity increases uniformly across all layers (Figure 7o).

4. Environmental Conditions Associated With Cold Pools

In this section, we examine the background environmental conditions associated with BLJ-related and non-BLJ-related cold pools across different convection systems, building upon their distinct characteristics outlined in Section 3.

Figure 8 shows the horizontal distributions of specific humidity and wind flow at 950 hPa during BLJ-related and non-BLJ-related cold pool events. For the BLJ-related cases, the maximum wind speeds exceed 9 m s^{-1} (Figures 8a and 8d), indicating stronger low-level winds compared to non-BLJ-related events, where the maximum wind speed is nearly 5–7 m s^{-1} (Figures 8b and 8e). The southwesterly BLJs transport abundant moisture from the South China Sea, resulting in higher environmental specific humidity near the coast and the Shenzhen Meteorological Tower (Figures 8a and 8d). Specifically, near the Shenzhen Meteorological Tower (the black rectangle), specific humidity in BLJ-related cold pools reaches approximately 18.3 g kg^{-1}, which is 0.5–1.0 g kg^{-1} higher than in non-BLJ-related events (Figures 8c and 8f). Under these wetter environmental conditions, the specific humidity in BLJ-related cold pools undergoes a greater reduction due to the descent of dry and cool air from the higher levels (Figures 2e, 6j and 7j). Simultaneously, strong southerly low-level winds impede the southward propagation of cold pools, resulting in a smaller increase in wind speed in BLJ-related cold pools (Figures 2b and 4), which is also observed in previous studies (e.g., Du et al., 2020; Wang et al., 2014). Figures 8a and 8b also highlight the noticeable influence of cold air in the northern South China, leading to substantial differences in ambient water vapor between BLJ-related and non-BLJ-related cold pools originating from MCSs (up to 1.0 g kg^{-1}), which further result in the distinct perturbations observed (Figure 6).

To gain a clearer understanding of horizontal moisture transportation by BLJs, we investigate the net moisture fluxes around the Shenzhen Meteorological Tower (black rectangle in Figure 8). The integrated vapor transports from the north, south, east, and west boundaries under different conditions are displayed in Figure 9. BLJ-related conditions exhibit significantly higher net moisture fluxes (1,647.5 kg s^{-1} for MCSs and 1,207.6 kg s^{-1} for individual convective cells, Figures 9a and 9c) compared to non-BLJ-related conditions (977.2 kg s^{-1} for MCSs and 832.3 kg s^{-1} for individual convective cells, Figures 9b and 9d). The difference in moisture fluxes between BLJ-related and non-BLJ-related cold pools is more pronounced for MCSs (670.3 kg s^{-1}), primarily resulting from variations in integrated vapor transport between the northern and southern boundaries during BLJ-related events (Figures 9a and 9c). These enhanced fluxes are attributed to elevated specific humidity and strong low-level winds.

Under the influence of warm southwesterly winds, positive temperature advection becomes more pronounced near the coasts, while inland areas experience cooling due to the intrusion of cold air from the north (not shown). This inland cooling, combined with higher specific humidity, jointly contributes to significantly enhanced relative humidity near the Shenzhen Meteorological Tower in BLJ-related environments, especially for cold pools by MCSs (red dots in a black rectangle in Figure 8c). However, the enhancement of environmental relative humidity associated with individual convective cells is less significant near the tower (red dots in a black rectangle in Figure 8f).

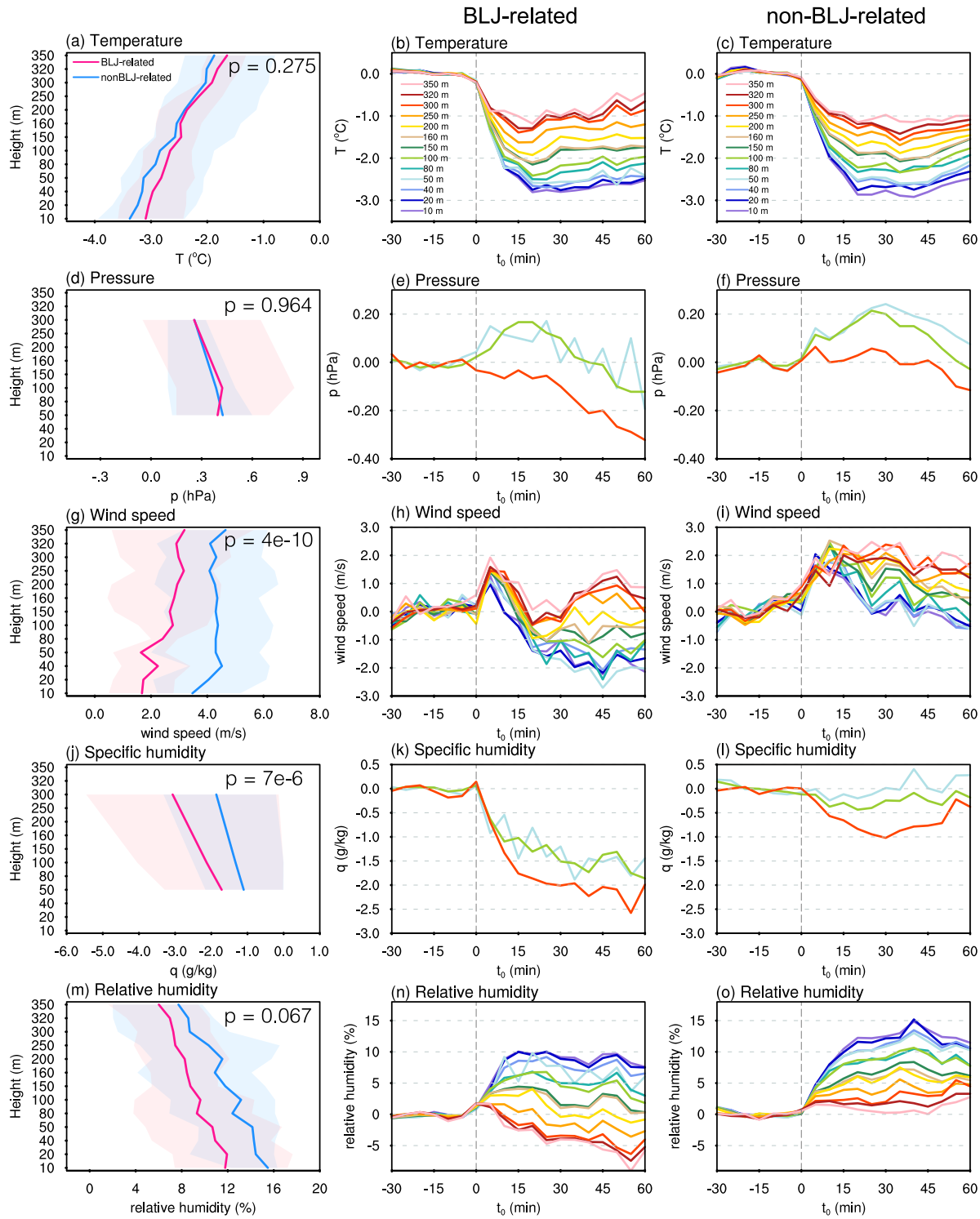

Figure 7. Same as Figure 6, but for cold pools generated from individual convective cells.

As a result, during BLJ-related events, the environment tends to be more humid, which reduces the potential for evaporative cooling and limits precipitation evaporation. This likely contributes to the weaker temperature drops and smaller pressure increases observed in BLJ-related cold pools, particularly those associated with MCSs. This observation is in agreement with the idea that the strength of the cold pool temperature signal is influenced by the pre-event evaporation potential or saturation deficit (Kirsch et al., 2021). In addition, strong low-level wind

Table 3
Mean Perturbation Values at Selected Heights for Non-BLJ-Related and BLJ-Related Cold Pools Generated From Individual Convective Cells

	Temperature (°C) (BLJ/non-BLJ)	Pressure (hPa) (BLJ/non-BLJ)	Wind speed (m/s) (BLJ/non-BLJ)	Specific humidity (g/kg) (BLJ/non-BLJ)	Relative humidity (%) (BLJ/non-BLJ)
10 m	−3.1/−3.4		1.7/3.5		11.8/15.5
50 m	−2.8/−3.1	0.4/0.4	1.6/4.3	−1.7/−1.1	10.7/14.1
100 m	−2.7/−2.8	0.4/0.4	2.8/4.4	−2.1/−1.3	9.6/13.2
300 m	−1.9/−2.0	0.3/0.3	3.0/4.3	−3.1/−1.9	7.3/8.7

speeds and humid environmental conditions enhance the energy exchange between cold pools and the surrounding atmosphere (Figure 5), further resulting in the shorter duration of cooling in BLJ-related cold pools.

5. Summary and Conclusion

In this study, we utilize multilevel observational data from the Shenzhen Meteorological Tower and ERA5 reanalysis data to investigate the impact of BLJs on cold pool characteristics during the pre-summer rainy season. Employing an objective identification method, we identify 54 cold pool events between April and June from 2018 to 2020, including 26 BLJ-related and 28 non-BLJ-related occurrences. The results reveal significant differences between these two types of cold pools, closely tied to the stronger wind speeds and more humid environments associated with BLJs.

Cold pools influenced by BLJs are generally weaker than those unrelated cold pools. On average, the near-surface (10-m) temperature drop is approximately 0.5°C smaller, the gust front wind speed increase is lower by over 1 m s^{-1}, and relative humidity rise is reduced by over 4%. In addition, the temperature drop in BLJ-related cold pools persists for a shorter duration (less by nearly 10 min). During the passage of cold pools, specific humidity decreases due to the transport of dry air from upper layers. This drying effect is more pronounced in BLJ-related cold pools, with a notable reduction of 0.9 g kg^{-1} greater than in non-BLJ-related cold pools. At higher altitudes,

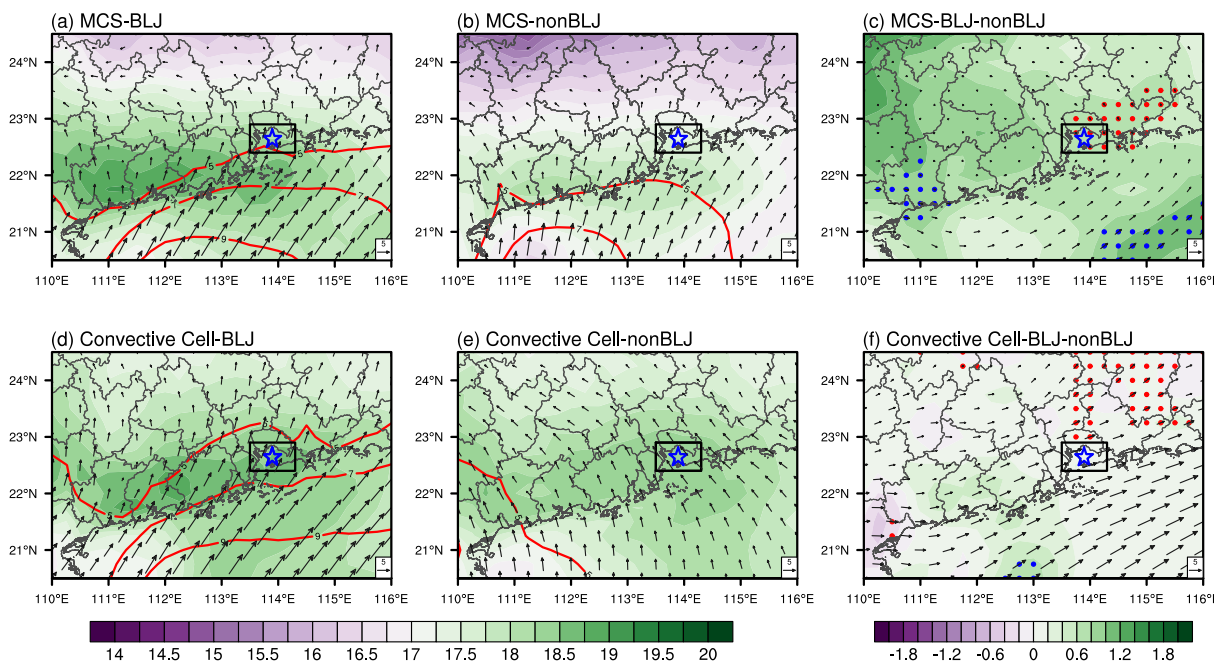

Figure 8. Specific humidity (shading; g kg^{-1}), horizontal wind speed (red contours; 5, 7 and 9 m s^{-1}), and wind vectors at 950 hPa for (a) BLJ-related and (b) non-BLJ-related cold pools and (c) the difference between the two types of cold pools from MCSs, and (d) BLJ-related and (e) non-BLJ-related cold pools and (f) the difference between the two types of cold pools from individual convective cells during the pre-summer rainy season. The black rectangle is used in Figure 8, and the blue star indicates the location of the Shenzhen Meteorological Tower. Blue (red) dots denote areas where the difference in specific (relative) humidity between BLJ-related and non-BLJ-related cold pools is statistically significant at the 90% level.

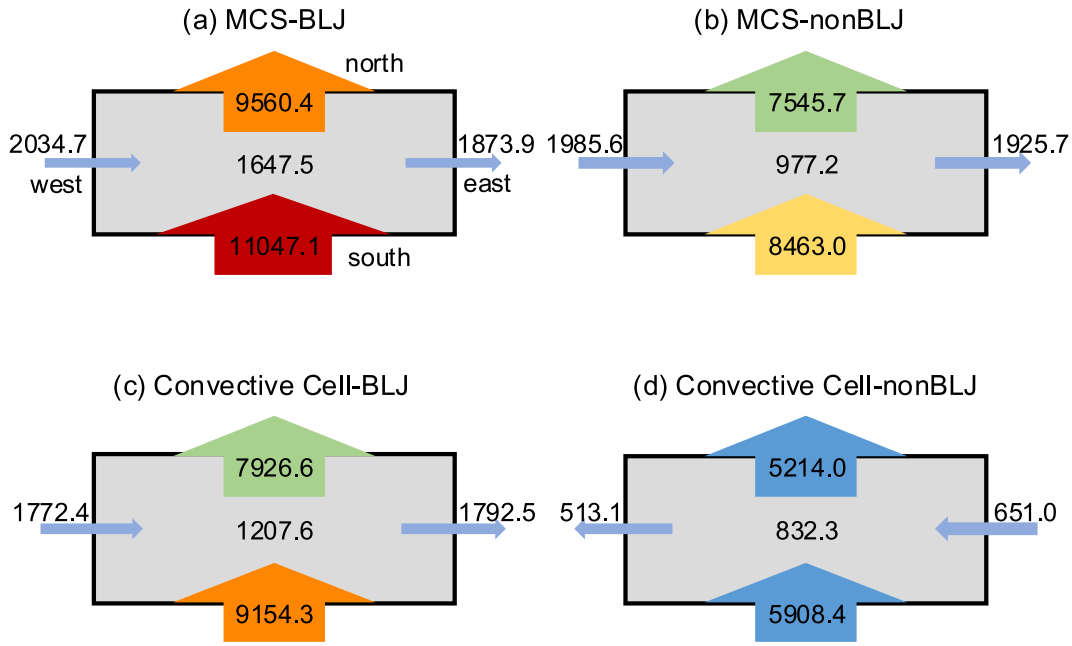

Figure 9. Net moisture flux and integrated vapor transport (kg s^{-1}) in the 900–1,000 hPa layer, showing fluxes from the north, south, west, and east for 24 hr before (a) BLJ-related and (b) non-BLJ-related cold pool events associated with MCSs and (c) BLJ-related and (d) non-BLJ-related cold pool events associated with individual convective cells during the pre-summer rainy season. The arrow colors qualitatively represent the magnitude of the variable, with warmer colors indicating larger values and cooler colors indicating smaller values.

the relative humidity in BLJ-related cold pools decreases over time, resulting from the marked decrease in specific humidity and smaller temperature drop. In contrast, at lower levels, relative humidity increases with time in both BLJ-related and non-BLJ-related cold pools. Furthermore, BLJ-related cold pools exhibit more significant variations in sensible heat flux, momentum flux, and TKE due to the strong wind shear associated with BLJs.

BLJ-related and non-BLJ-related cold pools generated by different types of convection, including MCSs and individual convective cells, are also compared. The cooling effects differs particularly pronounced in the two related cold pools from MCSs. In contrast, for individual convective cells, the difference in perturbations between BLJ-related and non-BLJ-related cold pools is relatively minor. However, the differences in wind speed and specific humidity signals of cold pools between with and without BLJs remain significant, even for cold pools from individual convective cells. Across all convective origins, statistically significant differences in wind speed and relative humidity consistently distinguish BLJ-related from non-BLJ-related cold pools, suggesting these two variables may serve as robust indicators for classification.

The surrounding environmental conditions are examined to further understand how BLJs influence cold pools. As shown in Figure 10, BLJs play a crucial role in moisture transport, with moist and warm air in the boundary layer near the coast primarily originating from the South China Sea and driven by the southwesterly BLJs. This leads to a higher relative humidity around the Shenzhen Meteorological Tower owing to increased moisture horizontal flux and vapor transport. Consequently, precipitation evaporation is suppressed under higher environmental humidity, resulting in weaker temperature drops but more pronounced drying within cold pools. These effects are especially evident in MCS-related events, where larger humidity contrasts between BLJ and non-BLJ environments intensify the observed differences. Additionally, the strong wind shear associated with BLJs enhanced turbulence, promoting greater energy and momentum exchange, which likely contributes to the shorter cooling duration of BLJ-related cold pools.

This study provides the first comprehensive examination of cold pool observations influenced by BLJs, revealing clear differences between BLJ-related and non-BLJ-related cold pools in South China. While the thermodynamic impacts of BLJs may vary regionally, the direct dynamical influence of BLJs, particularly through enhanced wind speeds, is likely relevant to cold pool behavior in other climatological settings. These multivariate distinctions

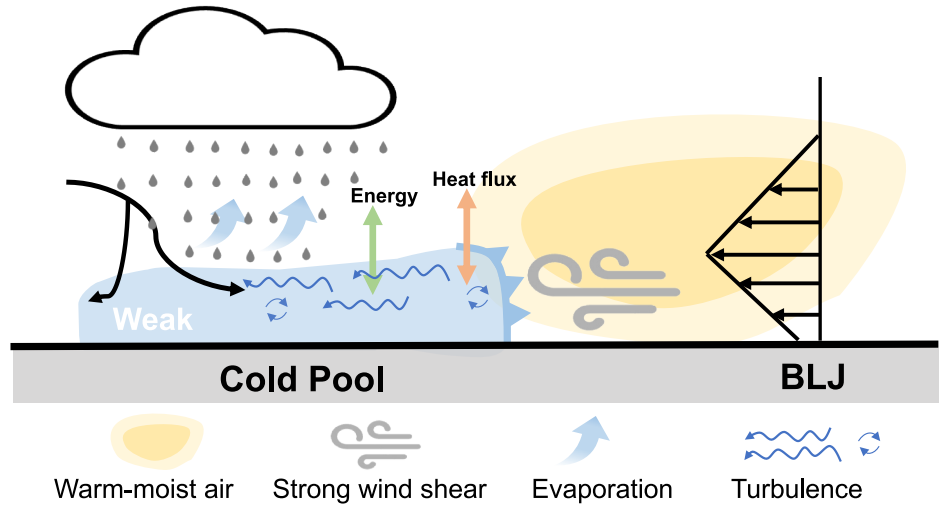

Figure 10. Schematic diagram of the impact of boundary layer jets on cold pools.

underscore the complex interactions between cold pools and boundary layer processes under the BLJs influence, offering valuable insights for improving numerical simulations of cold pool-BLJ interactions in subtropical regions. Nevertheless, gaps remain in understanding how the internal structure of cold pools evolves under the influence of BLJ and how these interactions impact convective organizations. Further investigation through idealized simulations is needed to address these questions.

Data Availability Statement

The observational data of radar are available at https://doi.org/10.5281/zenodo.15724815 (Fu, 2025). The ERA5 reanalysis data are from ECMWF via https://cds.climate.copernicus.eu/cdsapp#!/dataset/reanalysis-era5-pressure-levels?tab=overview (Hersbach et al., 2020). The tower data of cold pool events are from https://doi.org/10.5281/zenodo.14120603 (Fu, 2024).

Acknowledgments
This study was supported by the Guangdong Project of Basic and Applied Basic Research (Grants 2020B0301030004, 2025A1515011974, and 2024A1515510005), the National Natural Science Foundation of China (Grant 42475002), project supported by Southern Marine Science and Engineering Guangdong Laboratory (Zhuhai) (SML2024SP035, SML2024SP012, and 311024001), Heavy Rainfall Research Foundation of China (BYKJ2024Z01), and the Key Innovation Team of the China Meteorological Administration (CMA2023ZD08). We also acknowledge the high-performance computing support from the School of Atmospheric Sciences of Sun Yat-sen University.

References

Alduchov, O. A., & Eskridge, R. E. (1996). Improved Magnus form approximation of saturation vapor pressure. *Journal of Applied Meteorology*, *35*(4), 601–609. https://doi.org/10.1175/1520-0450(1996)035<0601:IMFAOS>2.0.CO;2

Bryan, G. H., Knievel, J. C., & Parker, M. D. (2006). A multimodel assessment of RKW theory's relevance to squall-line characteristics. *Monthly Weather Review*, *134*(10), 2772–2792. https://doi.org/10.1175/MWR3226.1

Chen, G., Sha, W., Iwasaki, T., & Wen, Z. (2017). Diurnal cycle of a heavy rainfall corridor over East Asia. *Monthly Weather Review*, *145*(8), 3365–3389. https://doi.org/10.1175/MWR-D-16-0423.1

Chowdhuri, S., Todekar, K., Murugavel, P., Karipot, A., & Prabha, T. V. (2021). Unravelling the turbulent structures of temperature variations during a gust front event: A case study. *Environmental Fluid Mechanics*, *21*(1), 263–281. https://doi.org/10.1007/s10652-020-09769-z

Drager, A. J., Grant, L. D., & Van Den Heever, S. C. (2020). Cold pool responses to changes in soil moisture. *Journal of Advances in Modeling Earth Systems*, *12*(8), e2019MS001922. https://doi.org/10.1029/2019MS001922

Du, Y., & Chen, G. (2018). Heavy rainfall associated with double low-level jets over southern China. Part I: Ensemble-based analysis. *Monthly Weather Review*, *146*(11), 3827–3844. https://doi.org/10.1175/MWR-D-18-0101.1

Du, Y., & Chen, G. (2019a). Climatology of low-level jets and their impact on rainfall over southern China during the early-summer rainy season. *Journal of Climate*, *32*(24), 8813–8833. https://doi.org/10.1175/JCLI-D-19-0306.1

Du, Y., & Chen, G. (2019b). Heavy rainfall associated with double low-level jets over southern China. Part II: Convection initiation. *Monthly Weather Review*, *147*(2), 543–565. https://doi.org/10.1175/MWR-D-18-0102.1

Du, Y., Chen, G., Han, B., Bai, L., & Li, M. (2020). Convection initiation and growth at the Coast of south China. Part II: Effects of the terrain, coastline, and cold pools. *Monthly Weather Review*, *148*(9), 3871–3892. https://doi.org/10.1175/MWR-D-20-0090.1

Du, Y., Shen, Y., & Chen, G. (2022). Influence of coastal marine boundary layer jets on rainfall in south China. *Advances in Atmospheric Sciences*, *39*(5), 782–801. https://doi.org/10.1007/s00376-021-1195-7

Du, Y., Zhang, Q., Chen, Y., Zhao, Y., & Wang, X. (2014). Numerical simulations of spatial distributions and diurnal variations of low-level jets in China during early summer. *Journal of Climate*, *27*(15), 5747–5767. https://doi.org/10.1175/JCLI-D-13-00571.1

Engerer, N. A., Stensrud, D. J., & Coniglio, M. C. (2008). Surface characteristics of observed cold pools. *Monthly Weather Review*, *136*(12), 4839–4849. https://doi.org/10.1175/2008MWR2528.1

Feng, Z., Hagos, S., Rowe, A. K., Burleyson, C. D., Martini, M. N., & Szoeke, S. P. (2015). Mechanisms of convective cloud organization by cold pools over tropical Warm Ocean during the AMIE/DYNAMO field campaign. *Journal of Advances in Modeling Earth Systems*, *7*(2), 357–381. https://doi.org/10.1002/2014MS000384

Foken, T., Göockede, M., Mauder, M., Mahrt, L., Amiro, B., & Munger, W. (2005). Post-Field data quality control. In X. Lee, W. Massman, & B. Law (Eds.), *Handbook of micrometeorology* (Vol. 29, pp. 181–208). Kluwer Academic Publishers. https://doi.org/10.1007/1-4020-2265-4_9
Fu, D. (2024). Shenzhen-Tower: Shenzhen-met (Shenzhen) [Dataset]. *Zenodo*. https://doi.org/10.5281/zenodo.14120604
Fu, D. (2025). The observational data of radar [Dataset]. *Zenodo*. https://doi.org/10.5281/zenodo.15724815
Gaal, R., Kinter, J. L., Dirmeyer, P. A., & Singh, B. (2024). Identifying the mechanism of interaction between soil moisture State and summertime MCS initiations in weakly forced synoptic environments using convective-permitting simulations. *Journal of Geophysical Research: Atmospheres*, *129*(23), e2024JD040855. https://doi.org/10.1029/2024JD040855
Gentine, P., Garelli, A., Park, S., Nie, J., Torri, G., & Kuang, Z. (2016). Role of surface heat fluxes underneath cold pools. *Geophysical Research Letters*, *43*(2), 874–883. https://doi.org/10.1002/2015GL067262
Goff, R. C. (1976). Vertical structure of thunderstorm outflows. *Monthly Weather Review*, *104*(11), 1429–1440. https://doi.org/10.1175/1520-0493(1976)104<1429:VSOTO>2.0.CO;2
Grant, L. D., Kirsch, B., Bukowski, J., Falk, N. M., Neumaier, C. A., Sakradzija, M., et al. (2024). How Variable Are Cold Pools? *Geophysical Research Letters*, *51*(6). https://doi.org/10.1029/2023gl106784
Grant, L. D., & Van Den Heever, S. C. (2016). Cold pool dissipation. *Journal of Geophysical Research: Atmospheres*, *121*(3), 1138–1155. https://doi.org/10.1002/2015JD023813
Han, Y., Liu, J., Sun, D., Han, F., Zhou, A., Zhao, R., et al. (2020). Fine gust front structure observed by coherent Doppler Lidar at Lanzhou Airport (103°49′ E, 36°03′ N). *Applied Optics*, *59*(9), 2686. https://doi.org/10.1364/AO.384634
He, J. Y., Chan, P. W., Li, Q. S., Li, L., Zhang, L., & Yang, H. L. (2022). Observations of wind and turbulence structures of super Typhoons Hato and Mangkhut over land from a 356 m high meteorological tower. *Atmospheric Research*, *265*, 105910. https://doi.org/10.1016/j.atmosres.2021.105910
Helfer, K. C., & Nuijens, L. (2021). The morphology of simulated trade-wind convection and cold pools under wind shear. *Journal of Geophysical Research: Atmospheres*, *126*(20), e2021JD035148. https://doi.org/10.1029/2021JD035148
Hersbach, H., Bell, B., Berrisford, P., Hirahara, S., Horányi, A., Muñoz-Sabater, J., et al. (2020). The ERA5 global reanalysis. *Quarterly Journal of the Royal Meteorological Society*, *146*(730), 1999–2049. https://doi.org/10.1002/qj.3803
Hitchcock, S. M., & Schumacher, R. S. (2020). Analysis of back-building convection in simulations with a strong low-level stable layer. *Monthly Weather Review*, *148*(9), 3773–3797. https://doi.org/10.1175/MWR-D-19-0246.1
International Electrotechnical Commission. (1999). Wind turbine generator systems-part 1: Safety requirements. IEC 61400-1.
Joseph, J., Girishkumar, M. S., McPhaden, M. J., & Rao, E. P. R. (2021). Diurnal variability of atmospheric cold pool events and associated air-sea interactions in the Bay of Bengal during the summer monsoon. *Climate Dynamics*, *56*(3–4), 837–853. https://doi.org/10.1007/s00382-020-05506-w
Khairoutdinov, M. F., Krueger, S. K., Moeng, C., Bogenschutz, P. A., & Randall, D. A. (2009). Large-Eddy simulation of maritime deep tropical convection. *Journal of Advances in Modeling Earth Systems*, *1*(4). JAMES.2009.1.15. https://doi.org/10.3894/JAMES.2009.1.15
Kirsch, B., Ament, F., & Hohenegger, C. (2021). Convective cold pools in long-term boundary layer mast observations. *Monthly Weather Review*, *149*(3), 811–820. https://doi.org/10.1175/MWR-D-20-0197.1
Kruse, I. L., Haerter, J. O., & Meyer, B. (2022). Cold pools over the Netherlands: A statistical study from tower and radar observations. *Quarterly Journal of the Royal Meteorological Society*, *148*(743), 711–726. https://doi.org/10.1002/qj.4223
Lan, C., Liu, H., Katul, G. G., Li, D., & Finn, D. (2019). Large eddies regulate turbulent flux gradients in coupled stable boundary layers. *Geophysical Research Letters*, *46*(11), 6090–6100. https://doi.org/10.1029/2019GL082228
Lan, C., Liu, H., Li, D., Katul, G. G., & Finn, D. (2018). Distinct turbulence structures in stably stratified boundary layers with weak and strong surface shear. *Journal of Geophysical Research: Atmospheres*, *123*(15), 7839–7854. https://doi.org/10.1029/2018JD028628
Lavers, D. A., Ralph, F. M., Waliser, D. E., Gershunov, A., & Dettinger, M. D. (2015). Climate change intensification of horizontal water vapor transport in CMIP5. *Geophysical Research Letters*, *42*(13), 5617–5625. https://doi.org/10.1002/2015GL064672
Li, H., Huang, Y., Hu, S., Wu, N., Liu, X., & Xiao, H. (2021). Roles of terrain, surface roughness, and cold pool outflows in an extreme rainfall event over the coastal Region of South China. *Journal of Geophysical Research: Atmospheres*, *126*(23), e2021JD035556. https://doi.org/10.1029/2021JD035556
Li, S., Meng, Z., & Wu, N. (2021). A preliminary study on the organizational modes of mesoscale convective systems associated with warm-sector heavy rainfall in south China. *Journal of Geophysical Research: Atmospheres*, *126*(16), e2021JD034587. https://doi.org/10.1029/2021JD034587
Li, X., & Du, Y. (2021). Statistical relationships between two types of heavy rainfall and low-level jets in south China. *Journal of Climate*, *34*(21), 18–8566. https://doi.org/10.1175/jcli-d-21-0121.1
Luo, Y., Wang, B., Wong, W. K., Hu, Z., Jou, B. J.-D., Lin, Y., et al. (2017). The Southern China Monsoon Rainfall Experiment (SCMREX). *Bulletin of the American Meteorological Society*, *98*(5), 999–1013. https://doi.org/10.1175/BAMS-D-15-00235.1
Mai, C., Du, Y., & Li, M. (2023). Processes of colliding cold pools derived from a 356-m-High Shenzhen met-tower during an extremely heavy rainfall event. *Monthly Weather Review*, *151*(6), 1571–1585. https://doi.org/10.1175/MWR-D-22-0214.1
Mai, C., Du, Y., Li, M., Chen, G., Su, L., Li, C., et al. (2025). Cold pools detected by a 356-m meteorological tower in a monsoon coastal region. *Advances in Atmospheric Sciences*. https://doi.org/10.1007/s00376-025-4446-1
Marion, G. R., & Trapp, R. J. (2019). The dynamical coupling of convective updrafts, downdrafts, and cold pools in simulated supercell thunderstorms. *Journal of Geophysical Research: Atmospheres*, *124*(2), 664–683. https://doi.org/10.1029/2018JD029055
Meng, W., Wang, A., Li, J., Fong, S., & Hou, E. (2004). Moist potential vorticity analysis of the heavy rainfall and mesoscale convective systems in South China. *Chinese Journal of Atmospheric Sciences*, *28*(3), 330–341. https://doi.org/10.3878/j.issn.1006-9895.2004.03.02
Parker, D. J. (1996). Cold pools in shear. *Quarterly Journal of the Royal Meteorological Society*, *122*(535), 1655–1674. https://doi.org/10.1002/qj.49712253509
Parker, M. D., & Johnson, R. H. (2000). Organizational modes of midlatitude mesoscale convective systems. *Monthly Weather Review*, *128*(10), 3413–3436. https://doi.org/10.1175/1520-0493(2001)129<3413:OMOMMC>2.0.CO;2
Pu, Y., Hu, S., Luo, Y., Liu, X., Hu, L., Ye, L., et al. (2022). Multiscale perspectives on an extreme warm-sector rainfall event over coastal south China. *Remote Sensing*, *14*(13), 3110. https://doi.org/10.3390/rs14133110
Purdom, J. F. W. (1976). Some uses of high-resolution GOES imagery in the mesoscale forecasting of convection and its behavior. *Monthly Weather Review*, *104*(12), 1474–1483. https://doi.org/10.1175/1520-0493(1976)104<1474:SUOHRG>2.0.CO;2
Ross, A. N., Tompkins, A. M., & Parker, D. J. (2004). Simple Models of the Role of Surface Fluxes in Convective Cold Pool Evolution. *Journal of the Atmospheric Sciences*, *61*(13), 1582–1595. https://doi.org/10.1175/1520-0469(2004)061<1582:smotro>2.0.co;2
Rotunno, R., Klemp, J. B., & Weisman, M. L. (1988). A theory for strong, long-lived squall lines. *Journal of the Atmospheric Sciences*, *45*(3), 463–485. https://doi.org/10.1175/1520-0469(1988)045<0463:ATFSLL>2.0.CO;2

Schiro, K. A., & Neelin, J. D. (2018). Tropical Continental downdraft characteristics: Mesoscale systems versus unorganized convection. *Atmospheric Chemistry and Physics*, *18*(3), 1997–2010. https://doi.org/10.5194/acp-18-1997-2018

Schlemmer, L., & Hohenegger, C. (2014). The formation of wider and deeper clouds as a result of cold-pool dynamics. *Journal of the Atmospheric Sciences*, *71*(8), 2842–2858. https://doi.org/10.1175/JAS-D-13-0170.1

Schlemmer, L., & Hohenegger, C. (2015). Modifications of the atmospheric moisture field as a result of cold-pool dynamics. *Quarterly Journal of the Royal Meteorological Society*, *142*(694), 30–42. https://doi.org/10.1002/qj.2625

Simoes-Sousa, I. T., Tandon, A., Buckley, J., Sengupta, D., J, S. L., Shroyer, E., & De Szoeke, S. P. (2022). Atmospheric cold pools in the Bay of Bengal. *Journal of the Atmospheric Sciences*. https://doi.org/10.1175/JAS-D-22-0041.1

Su, L., Sun, X., Du, Y., Fung, J. C. H., & Chen, G. (2023). The roles of local convergences in the convection initiation of a record-breaking rainfall event at the coastal pearl river Delta in south China. *Journal of Geophysical Research: Atmospheres*, *128*(3), e2022JD037234. https://doi.org/10.1029/2022JD037234

Thorpe, A. J., Miller, M. J., & Moncrieff, M. W. (1982). Two-dimensional convection in non-constant shear: A model of mid-latitude squall lines. *Quarterly Journal of the Royal Meteorological Society*, *108*(458), 739–762. https://doi.org/10.1002/qj.49710845802

Tompkins, A. M. (2001). Organization of tropical convection in low vertical wind shears: The role of cold pools. *Journal of the Atmospheric Sciences*, *58*(13), 1650–1672. https://doi.org/10.1175/1520-0469(2001)058<1650:OOTCIL>2.0.CO;2

Torri, G., Kuang, Z., & Tian, Y. (2015). Mechanisms for convection triggering by cold pools. *Geophysical Research Letters*, *42*(6), 1943–1950. https://doi.org/10.1002/2015GL063227

van den Heever, S. C., Grant, L. D., Freeman, S. W., Marinescu, P. J., Barnum, J., Bukowski, J., et al. (2021). The Colorado state university convective CLoud outflows and UpDrafts experiment (C3LOUD-Ex). *Bulletin of the American Meteorological Society*, *102*(7), E1283–E1305. https://doi.org/10.1175/BAMS-D-19-0013.1

Vogel, R., Konow, H., Schulz, H., & Zuidema, P. (2021). A climatology of trade-wind cumulus cold pools and their link to mesoscale cloud organization. *Atmospheric Chemistry and Physics*, *21*(21), 16609–16630. https://doi.org/10.5194/acp-21-16609-2021

Wang, D., Giangrande, S. E., Schiro, K. A., Jensen, M. P., & Houze, R. A. (2019). The characteristics of tropical and midlatitude mesoscale convective systems as revealed by radar wind profilers. *Journal of Geophysical Research: Atmospheres*, *124*(8), 4601–4619. https://doi.org/10.1029/2018JD030087

Wang, H., Luo, Y., & Jou, B. J. (2014). Initiation, maintenance, and properties of convection in an extreme rainfall event during SCMREX: Observational analysis. *Journal of Geophysical Research: Atmospheres*, *119*(23). https://doi.org/10.1002/2014JD022339

Weisman, M. L., Klemp, J. B., & Rotunno, R. (1988). Structure and evolution of numerically simulated squall lines. *Journal of the Atmospheric Sciences*, *45*(14), 1990–2013. https://doi.org/10.1175/1520-0469(1988)045<1990:saeons>2.0.co;2

Xie, J., Lan, C., Yang, H., Gao, R., Lu, C., Wang, B., et al. (2022). Tower-observed structural evolution of the low-level boundary layer before, during, and after gust front passage in a coastal area at low latitude. *Weather and Climate Extremes*, *36*, 100429. https://doi.org/10.1016/j.wace.2022.100429

Xu, B., Lang-ming, Y., Xian-tong, L., Xiao-na, R., Hui, X., Jia-min, X., et al. (2023). Thermodynamics and microphysical characteristics of an extreme rainfall event under the influence of a low-level jet over the south China Coast. *Journal of Tropical Meteorology*, *29*(1), 216–235. https://doi.org/10.46267/j.1006-8775.2023.017

Zhang, J., Bai, L., Li, Z., Du, Y., & Zhang, S. (2023). High-frequency microbarograph-observed pressure variations associated with gust fronts during an extreme rainfall event. *Remote Sensing*, *16*(1), 101. https://doi.org/10.3390/rs16010101

Zhang, M., Rasmussen, K. L., Meng, Z., & Huang, Y. (2022). Impacts of coastal terrain on warm-sector heavy-rain-producing MCSs in southern China. *Monthly Weather Review*, *150*(3), 603–624. https://doi.org/10.1175/MWR-D-21-0190.1

Zipser, E. J. (1977). Mesoscale and convective–scale downdrafts as distinct components of squall-line structure. *Monthly Weather Review*, *105*(12), 1568–1589. https://doi.org/10.1175/1520-0493(1977)105<1568:MACDAD>2.0.CO;2